EvaSurf: Efficient View-Aware Implicit Textured Surface Reconstruction on Mobile Devices

Jingnan Gao
Shanghai Jiao Tong University
gjn0310@sjtu.edu.cn

Zhuo Chen
Shanghai Jiao Tong University
ningci5252@sjtu.edu.cn

Yichao Yan
Shanghai Jiao Tong University
yanyichao@sjtu.edu.cn

Bowen Pan
Alibaba Group
bowen.pbw@alibaba-inc.com

Zhe Wang
Alibaba Group
xingmi.wz@alibaba-inc.com

Jiangjing Lyu
Alibaba Group
jiangjing.ljj@alibaba-inc.com

Xiaokang Yang
Shanghai Jiao Tong University
xkyang@sjtu.edu.cn

Synthetic Data   **Real-World Data**

Ground Truth   **Rendering**   **Mesh**   **Ground Truth**   **Rendering**   **Mesh**   **Real-Time Rendering**
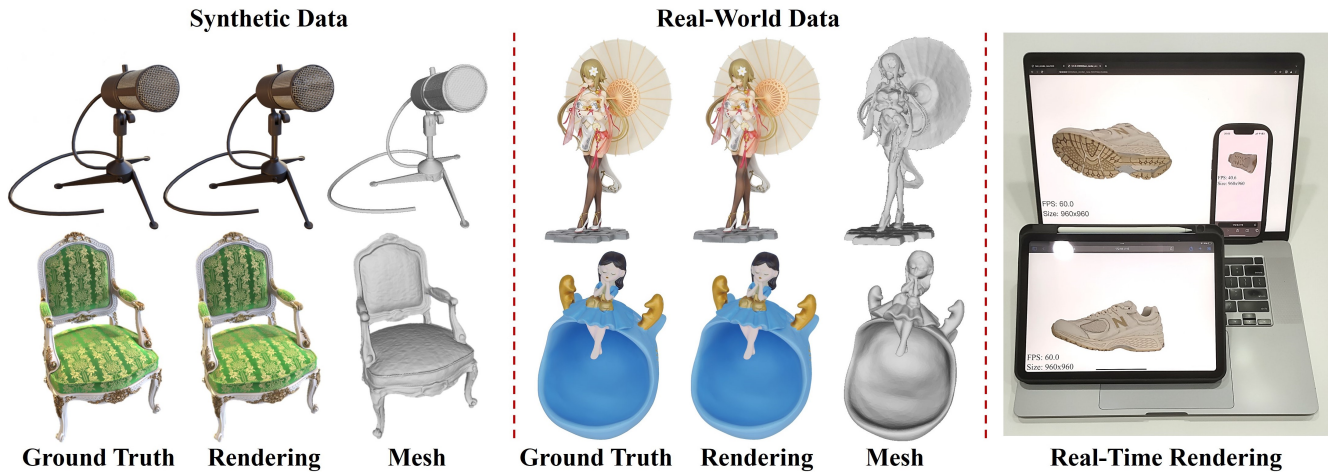
Figure 1. Examples of reconstruction results of **EvaSurf**. Our model can reconstruct the high-quality appearance and accurate mesh on various devices in real-time for both synthetic and real-world objects.

Abstract

*Reconstructing real-world 3D objects has numerous applications in computer vision, such as virtual reality, video games, and animations. Ideally, 3D reconstruction methods should generate high-fidelity results with 3D consistency in real-time. Traditional methods match pixels between images using photo-consistency constraints or learned features, while differentiable rendering methods like Neural Radiance Fields (NeRF) use differentiable volume rendering or surface-based representation to generate high-fidelity scenes. However, these methods require excessive runtime for rendering, making them impractical for daily applications. To address these challenges, we present **Eva-Surf**, an **E**fficient **V**iew-**A**ware implicit textured **Surf**ace re-construction method on mobile devices. In our method, we first employ an efficient surface-based model with a multi-view supervision module to ensure accurate mesh reconstruction. To enable high-fidelity rendering, we learn an implicit texture embedded with a set of Gaussian lobes to capture view-dependent information. Furthermore, with the explicit geometry and the implicit texture, we can employ a lightweight neural shader to reduce the expense of computation and further support real-time rendering on common mobile devices. Extensive experiments demonstrate that our method can reconstruct high-quality appearance and accurate mesh on both synthetic and real-world datasets. Moreover, our method can be trained in just 1-2 hours using a single GPU and run on mobile devices at over 40 FPS (Frames Per Second), with a final package required*

for rendering taking up only 40-50 MB. Our project website is at: https://g-1nonly.github.io/EvaSurf-Website/

1. Introduction

3D reconstruction has long been an essential task in computer graphics and computer vision, with broad potentials in the area of VR/AR, video games, and film industry [1, 18, 25]. To support the generalized applications, it is desirable for an ideal 3D reconstruction method to have the following properties: (1) **High efficiency** that supports real-time rendering for 3D objects on various devices including PCs, tablets, and mobile phones; (2) **Realistic rendering** that faithfully reflects the appearance of original objects with multi-view consistency; (3) **Accurate geometry** that provides a detailed mesh to be flexibly edited and manipulated by users with modern software.

Recently, neural rendering methods [4, 26–30, 32, 35, 36, 40, 46, 51, 56, 64, 67] have emerged as a promising solution because they achieve high-fidelity rendering results from multi-view images. However, traditional NeRF-based methods [30, 32, 38, 56, 66] require plenty of sampling points to forward a deep MLP network, requiring massive computation that is impractical for mobile devices. To improve the efficiency of neural rendering, current methods [9, 17] usually store the opacity and texture using representations that simplify the sampling process of the neural radiance field. While these methods achieve efficient and photo-realistic rendering on mobile devices, they suffer from the limitation in capturing accurate geometry as the continuous implicit function cannot provide explicit information about the underlying geometry of the object. To obtain accurate geometry, the following works [43, 44, 47, 62] for efficient rendering adopt surface-based methods that learn an implicit-explicit hybrid representation and then bake it into meshes. Despite the improvement in geometry, they are still insufficient to obtain accurate meshes with smooth and solid surfaces regarding complex structures or non-Lambertian surfaces. Besides, due to the entangled learning of appearance and material, it is also difficult for these methods to render regions with view-dependent effects such as specularities.

Based on the above discussions, it is natural to ask a question: can we build a model that solves the mentioned challenges and meanwhile satisfies all three requirements, *i.e.*, high efficiency, realistic rendering, and accurate geometry? In this work, we present **EvaSurf**, an **E**fficient **V**iew-**A**ware implicit textured **Surf**ace reconstruction method on mobile devices. As the joint learning for the geometry and appearance may lead to entangled attributions, we design a two-stage framework to respectively reconstruct the geometry and appearance. **(1)** In the first stage, we employ an efficient surface-based model with a multi-view supervision module to learn accurate structures of geometry. **(2)** In the second stage of appearance reconstruction, the view-dependent effect severely influences the quality of rendering images. Therefore, we incorporate a set of Gaussian lobes into an implicit texture, to assign different weights to the dimensions of the view-aware texture, thus modeling the appearance with view-dependent effects. **(3)** With the explicit geometry and the learned implicit texture, we show that a lightweight neural shader is sufficient to achieve high-quality differentiable rendering. The small size of the neural shader can greatly reduce the consumption of computation and memory sources, empowering real-time rendering on mobile devices.

With the help of proposed strategies, the training procedure of our method can be completed in just 1-2 hours on a single GPU, 10× faster than MobileNeRF [9]. The inference rendering can be performed on common mobile devices at a speed of at least 40 FPS (Frames Per Second), and the final storage of rendering packages only takes up 40-50 MB (Megabytes), much smaller than existing methods [9, 44, 47]. Moreover, as depicted in Fig. 1, our method can not only handle synthetic data but also reconstruct high-quality results on complex real-world objects.

In summary, our framework, EvaSurf:
- proposes a two-step framework to achieve efficient, high-quality 3D reconstruction while obtaining accurate mesh;
- models the view-dependent appearance by incorporating the Gaussian lobes into an implicit texture;
- runs on common devices including PCs, tablets, and mobile phones with over 40 FPS and trains in 1-2 hours while consuming much smaller disk storage of the rendering package than existing methods.

2. Related Work

2.1. Neural Rendering for 3D Reconstruction

To ensure the consistency of reconstructed 3D objects, multi-view methods [5, 6, 8, 15, 24, 50, 53] use geometry representations like point clouds and depth maps to extract the corresponding mesh. Later methods [10, 14, 19, 22, 34, 45] estimate the mesh by optimizing an initial mesh based on photo consistency. Furthermore, learned features and neural shape priors were introduced [23, 57, 58] for mesh deformation. These methods often rely on strict assumptions or priors to ensure 3D consistency, which cannot yield high-fidelity results for varying light conditions.

More recently, neural rendering technique has been widely adopted in the field of 3D object reconstruction. Incorporating the implicit representations, Neural Radiance Field (NeRF) [32] and its followers [2, 3, 7, 12, 16, 30, 33, 35, 40, 42, 56] achieve high-fidelity rendering results. These methods incorporate ray-marching and ray-sampling
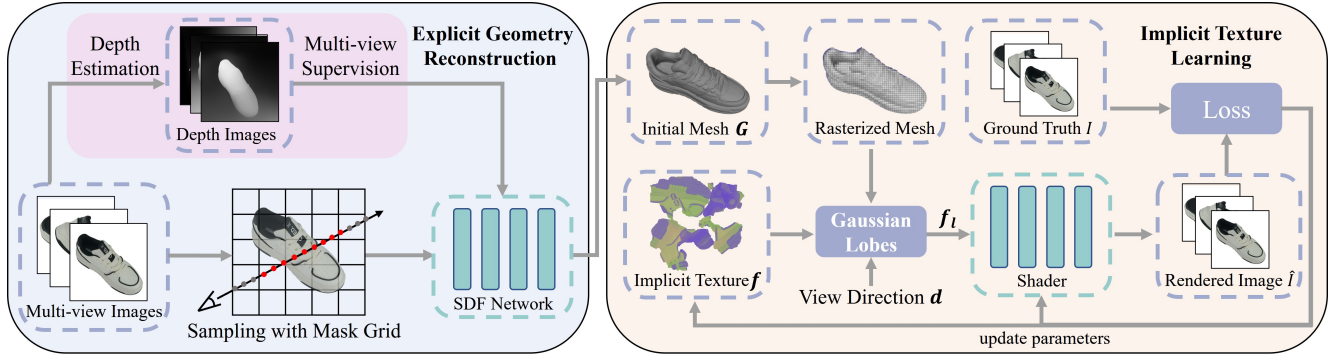
Figure 2. **The overview of our full pipeline**. We begin with an initial explicit geometry generated by a surface-based model. We then rasterize the mesh and utilize a set of Gaussian lobes to embed the view-dependent information into a learnable implicit texture. Given the geometry and texture, a neural shader renders the final RGB images.

mechanisms during the process of neural rendering through an encoded 5D continuous field. The neural network estimates volume densities and RGB values along the sampled points on the marching rays. However, the corresponding geometry reconstructed by these methods is not satisfactory and accurate due to the ambiguity of volume rendering. To improve the quality of geometry, surface-based rendering methods open up another road for 3D reconstruction. These methods optimize the underlying surface directly, or gradually deform the geometry from volumetric representation into a surface representation. The implicit surface representations are encoded in neural networks such as occupancy networks [31, 36, 37, 39] or neural signed distance functions [11, 13, 21, 36, 37, 52, 54, 59–61, 63, 65]. Although these methods are able to generate relatively satisfactory geometry and appearance, they often require excessive runtime and thus become impractical for daily real-time applications. Conversely, our method also adopts neural rendering for the appearance but uses explicit mesh to represent the geometry, which is integrated into an efficient two-stage framework and supports real-time rendering.

2.2. Real-time Rendering on Mobile Devices

With the rapid development of modern technology, mobile phones, and other mobile devices have become an essential part of people's daily lives. Real-time rendering on these devices has emerged as an important research topic. Before the introduction of neural radiance fields, several methods [48, 49, 55] employ a neural texture and a neural renderer to render a scene. Though these methods can achieve photo-realistic rendering in real time, they may not be generalized to arbitrary 3D objects due to their requirements of geometry priors. To facilitate the power of NeRF to render scenes on mobile devices, Hedman *et al.* [17] propose a solution that bakes NeRF into sparse neural radiance grids (SNeRG). However, the rendering speed of SNeRG fails to achieve real-time performance, hindering the attain-

ment of interactive rendering rates. In contrast, MobileN-eRF [9] adopts textured polygons as the scene representation and leverages the polygon rasterization pipeline to accelerate the rendering process. Although MobileNeRF supports real-time rendering with interactive frame rates, the exported mesh may be inaccurate due to its complex interlacing polygons. Re-ReND [44] and NeRF2Mesh [47] both train a NeRF-like model at the initial stage and then bake the appearance into a texture map and extract the corresponding mesh. Nevertheless, these methods [41, 44, 47] are unable to render scenes with view-dependent effects and can not reconstruct accurate mesh for complex structures and non-Lambertian objects. Bakedsdf [62] utilizes a hybrid SDF-volume representation and bakes the representation into meshes for real-time rendering. However, it tends to learn over-smooth surfaces and cannot handle complex structures. In comparison, our method employs a multi-view supervision module that allows the surface-based model to learn the complex structure and prevent the model from over-smoothing. We also introduce a set of Gaussian lobes to embed view-dependent information in feature space for more realistic renderings.

3. Methods

Given a set of images $\mathcal{I} = \{I_1, ..., I_n\}$, we aim to optimize a representation to efficiently synthesize novel views and generate accurate mesh at interactive frame rates. To this end, we design a two-stage differentiable framework that requires much less computation and disk storage so as to make it compatible with mobile devices. As depicted in Fig. 2, we first utilize a surface-based model $\mathcal{S}$ to reconstruct an accurate geometry (3.1). In the second stage, we rasterize the initial mesh and introduce a set of Gaussian lobes L to embed the view-dependent information into an implicit texture f (3.2). Finally, we jointly optimize the implicit texture f and a neural shader, *i.e.*, a lightweight MLP,

which takes the view-embedded implicit feature f_l as input and directly outputs the rendered images $\hat{I}$ (3.3).

3.1. Efficient Explicit Geometry Reconstruction

As the base of the reconstruction pipeline, an accurate geometry is crucial for the following high-quality rendering. To overcome the challenge of coarse geometry faced by the traditional NeRFs, our model first trains a surface-based model $\mathcal{S}$ that leverages a set of signed distance function (SDF) to directly estimate the explicit geometry (mesh). However, previous surface-based models usually require excessive training time and struggle to generate accurate results for objects with complex structures. Therefore, we design two additional strategies to further solve these challenges. To tackle the issue of low-speed training, as depicted in Fig. 2, we employ a set of spatial grids with mask to filter the sampled points during the learning process, enabling the model to converge within 2 hours (**5× faster than Neus [54]**). It is noteworthy that employing spatial grids at low resolution may lead to smooth but coarse mesh results, while high-resolution grids might induce overfitting. In order to generate an accurate geometry without introducing additional noise, we utilize a set of progressive grids $g(\beta)$ that gradually increase the bandwidth to realize the coarse-to-fine training strategy. The set of progressive grids can be formulated as follows:

$$g(\beta) = (w_1(\beta)g_1, w_2(\beta)g_2, ..., w_l(\beta)g_l), \quad (1)$$

where β is a parameter determined empirically to modulate the bandwidth and g_i is the multi-resolution spatial grids at level-i with corresponding weight indicator $w = I(i \leq \beta)$.

Moreover, to improve the quality of the geometry, we introduce a multi-view supervision (MVS) module that renders depth images to supervise the surface-based model learning. This module can prevent our model from generating over-smooth surfaces and encourage it to learn complex structures. Overall, for an explicit geometry G represented by triangle mesh with vertex positions V, the objective is:

$$\underset{V, \theta}{\arg\min} \left(\mathcal{L}_s(G) + \mathcal{L}_{mvs}(G) \right), \quad (2)$$

where θ is the parameters to be optimized, $\mathcal{L}_s$ is the loss of the surface-based model and $\mathcal{L}_{mvs}$ is the loss of the multi-view supervision module. The details of the loss will be discussed in the *supplementary material*.

In contrast to the mesh generated by MobileNeRF [9], which is produced through the intersection of interlaced polygons, our obtained mesh can be directly unwrapped into UV form and can be edited directly without further operation in contemporary software packages. Compared to previous methods [44, 47] that extract a mesh from a trained NeRF model, our method can generate an explicit mesh
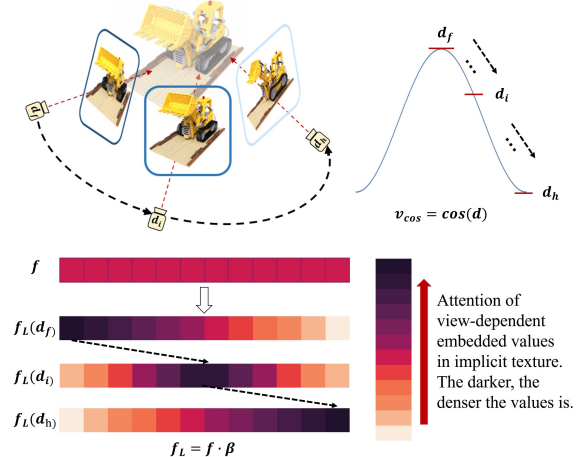

Figure 3. View-dependent embedded mechanism in feature space. We equip our model with a set of Gaussian lobes to capture the view-dependent information. The heatmap demonstrates the corresponding relation between the values and the view direction.

with clearly defined boundaries and high accuracy. The normal information obtained from the explicit mesh is utilized for subsequent improvement in the texture training stage, establishing a robust foundation for the overall pipeline.

3.2. View-aware Implicit Texture

In current frameworks [44, 47], the reconstruction of appearance is usually achieved by directly baking the appearance into texture maps. While these methods manage to render photo-realistic scenes on mobile devices, they struggle to model the view-dependent appearances. As a result, specularities are usually interpreted as virtual lights on the surface of the object, leading to inaccurate renderings. Intuitively, a point is expected to exhibit varying colors when observed from different view directions. To model such view-dependent effects, we equip our texture map with a set of Gaussian lobes, assigning different weights to the texture feature for various views, as depicted in Fig. 3.

However, applying Gaussians at the stage of ray sampling or positional encoding usually requires additional computation, preventing our model from efficient rendering on mobile devices. Therefore, unlike Mip-NeRF [2] that employs Gaussians to approximate the conical frustums on the 3D point level, our method instead utilizes the set of **Gaussians lobes on the feature-level**. Specifically, to encourage the model to learn view-dependent effects, given an initialized geometry G, we first decimate the mesh and perform vertex processing that rasterizes the mesh and stores the vertex indices and barycentric coordinates (u, v) associated with each pixel. Normals $n \in \mathbb{R}^3$ can then be calculated at each position. Given a view direction $d \in \mathbb{R}^3$, we specifically calculate a cosine vector v_{cos} that represents the

angle between the view direction d and the normals n, serving for the following view-dependent computation:

$$v_{cos} = \frac{-d \cdot n}{\|d\| \cdot \|n\|}. \tag{3}$$

Furthermore, we employ a set of Gaussian lobes to incorporate the view-dependent information, *i.e.*, specularities, into the texture:

$$L(f, v_{cos}) = f \cdot \left(\frac{1}{\alpha \sqrt{2\pi}} e^{-\frac{(v_{cos}-t)^2}{2\alpha^2}} \right), \tag{4}$$

where f is the learnable implicit texture which is a 12-dimensional feature map initialized with random Gaussian noise, α is a hyper-parameter and t is a 12-dimensional constant vector to indicate the channel number. It is noteworthy that we employ a learnable 12-dimensional implicit texture in our pipeline to contain more detailed information, stored as three *PNG* images with four channels for convenience.

With the introduction of the Gaussian lobes, our method encodes the view-dependent information in the feature space instead of the 3D point space. Specifically, the view-dependent information is represented as the concentration of the values in the texture map. By assigning different weights to each dimension of the texture, we model view dependence with different fidelity and thus encourage the texture to learn the view-dependent information in the scene. For example, a cosine value of 1 ($\cos(0)$) corresponds to a frontal view, with the attention of values lying at the front of the implicit texture. In this way, our method is able to generate a range of view-dependent effects and improve the quality of the rendered images.

3.3. Light-weight Neural Shader

In our two-stage framework mentioned above, we utilize an efficient surface-based model to learn the explicit geometry and employ an implicit texture to model the appearance. With the explicit geometry and the implicit texture, the neural shader can be extremely light. This is because its function is just to connect the view-aware texture with the RGB values, instead of computing the features representing the geometry and fitting the RGB values from the inputs, as the large MLP used in NeRF [32]. Therefore, our framework utilizes a much smaller MLP than the original NeRF model, which significantly reduces the computation expense and storage resources, enabling real-time rendering on mobile devices.

The overall shading process can be summarized as follows. Given the view-embedded implicit texture $f_l = L(f, v_{cos})$, where v_{cos} represents the cosine vector, L represents the set of Gaussian lobes, and f represents the implicit texture, our framework optimizes a neural shader $Shader_\theta$, which is a lightweight MLP for the reconstruction of the 3D

objects. The pipeline can be formulated as:

$$I = Shader_\theta(f_l), \tag{5}$$

where I represents the rendered image.

3.4. Differentiable Training

Similar to [20], we adopt the differentiable rendering technique for the training procedure. As depicted in Fig. 2, during the forward-pass procedure, our method renders a 2D image given the explicit geometry and the learnable implicit texture, which altogether affect the shape and appearance of a 3D object. As for the backward-pass stage, the gradient of the loss with respect to the input shape and appearance factors is computed given the gradient of the loss function defined on the output image pixels. Here, we use the *L2* loss to measure reconstruction loss:

$$\mathcal{L} = \|\hat{C} - C_{gt}\|_2^2, \tag{6}$$

where $\hat{C}$ represents the predicted RGB value and C_{gt} represents the ground truth value. Therefore, the derivation of the backward-pass stage could be formulated as:

$$\frac{\partial \mathcal{L}}{\partial \{x, y, z, w\}} = \frac{\partial \mathcal{L}}{\partial \{u, v\}} \cdot \frac{\partial \{u, v\}}{\partial \{x, y, z, w\}}, \tag{7}$$

where (x, y, z, w) is the homogeneous coordinates input from the world space and (u, v) is the barycentric coordinates from the image space.

4. Experiments

4.1. Experiment Setups

In our experiments, we mainly use two datasets:
Synthetic Dataset. We evaluate the performance on the 8 synthetic 360° scenes from NeRF [32]. It consists of 8 path-traced scenes with 100 images for training and 200 images for testing per scene.
Real-world Dataset. To demonstrate the effectiveness of our method, we also construct a set of real-world high-resolution (**2K**) data. This dataset comprises **15 objects**, with each object consisting of over 200 images. These images are captured by **accurate camera poses**, facilitating precise correlation between the data and the corresponding imaging parameters.

4.2. Comparisons on Synthetic Data

Geometry Quality. To evaluate the geometry quality, we compare the exported meshes of our method and previous methods [9, 34, 44, 47, 54]. We choose bi-directional Chamfer Distance as the evaluation metric. Nevertheless, due to the fact that the ground truth meshes may not accurately represent surface meshes, we cast rays and sample 2.5 million points from the intersections between the
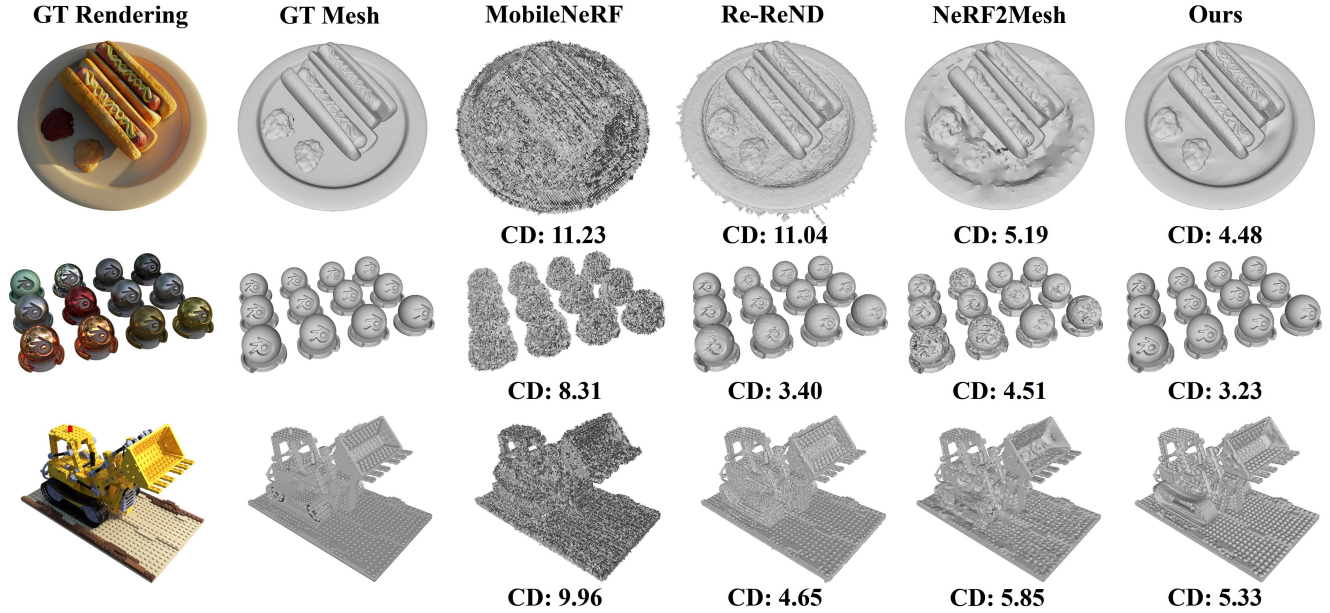
Figure 4. Comparison of generated mesh on NeRF synthetic dataset. Our method generates more accurate meshes compared with previous methods, especially for objects where view-dependent effects occur. The Chamfer Distance ↓ (the unit is 10^{-3}) results are also provided.

	Mobile	Chair	Drums	Ficus	Hotdog	Lego	Materials	Mic	Ship	Mean
NeuS [54]	✗	**3.95**	6.68	2.84	8.36	6.62	4.10	2.99	9.54	5.64
NVdiffrec [34]	✗	4.13	8.27	5.47	7.31	5.78	4.98	3.38	25.89	8.15
MobileNeRF [9]	✓	7.82	9.49	8.98	11.23	9.96	8.31	9.61	15.23	10.08
Re-ReND [44]	✓	3.96	-	5.60	11.04	**4.65**	3.40	-	-	-
NeRF2Mesh [47]	✓	4.60	**6.02**	**2.44**	5.19	5.85	4.51	3.47	8.39	5.06
Ours	✓	4.16	6.97	2.72	**4.48**	5.33	**3.23**	**2.83**	**5.41**	**4.39**

Table 1. Comparison of Chamfer Distance ↓ on NeRF synthetic dataset (the unit is 10^{-3}). We use "Mobile" to denote whether a method supports rendering on mobile devices or not. Our method achieves better surface reconstruction quality compared to previous methods while supporting real-time rendering on mobile devices. Note that Re-ReND [44] extracts a mesh before the rendering pipeline but some of the meshes are not provided, so we only evaluated the meshes provided by the authors.

rays and the surfaces in each scene following the evaluation process of [47]. The quantitative results are demonstrated in Table 1. Compared with previous methods for surface reconstruction [34, 54], our method achieves superior mesh quality while supporting real-time rendering on mobile devices. Compared with existing methods [9, 44, 47] that allow rendering on mobile devices, our method has the ability to generate more accurate mesh for the scenes with view-dependent effects. As depicted in Fig. 4, our model demonstrates the capability to reconstruct smoother surfaces for non-Lambertian objects (*Materials*). Additionally, we achieve more consistent mesh results when facing objects affected by environmental lighting conditions, such as *Lego* and *Hotdog*. The underlying reason for the improvements can be attributed to the explicit mesh with multi-view supervision employed for obtaining the geometry. Specif-

ically, MobileNeRF [9] synthesizes a mesh from the area constructed by interlacing polygons, leading to an inaccurate mesh with ambiguous boundaries. Re-ReND [44] and NeRF2Mesh [47] both train a NeRF-like model first and then extract mesh from the model. However, these NeRF-based models tend to interpret the view-dependent effects as virtual lights underneath the actual surfaces, leading to inaccurate mesh results. Meanwhile, by utilizing an explicit geometry, our method can learn a solid mesh with a smooth surface. Therefore, we surpass previous methods by generating accurate meshes for a greater variety of objects.

Rendering Quality. To evaluate the performance of rendering quality, we compare our results with the state-of-the-art methods that achieve real-time rendering on mobile devices [9, 44, 47]. We also provide the results of the original NeRF model [32] and SNeRG [17] as reference. We choose
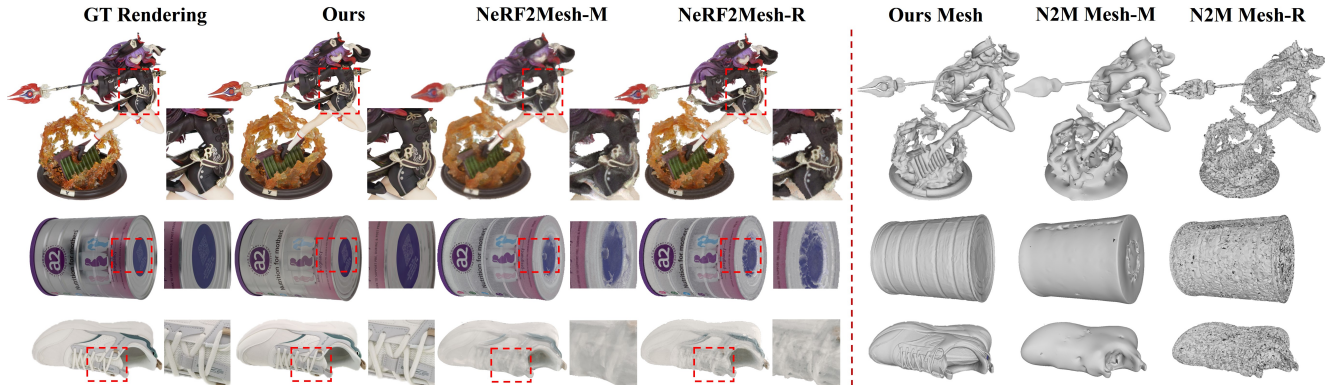
Figure 5. Results on real-world dataset. Our method can reconstruct 3D objects from the real-world dataset with high-fidelity rendered results and more accurate mesh than the existing methods. We denote the NeRF2Mesh [47] better mesh setting as "N2M Mesh-M" and better rendering setting as "N2M Mesh-R" in the figure.

	PSNR ↑	SSIM ↑	LPIPS ↓
NeRF [32]	31.01	0.947	0.081
SNeRG [17]	30.38	0.950	0.050
MobileNeRF [9]	30.90	0.947	0.062
Re-ReND [44]	29.00	0.934	0.080
NeRF2Mesh(R) [47]	31.04	0.948	0.066
NeRF2Mesh(M) [47]	29.76	0.940	0.072
Ours	30.03	0.944	0.070

Table 2. Quantitative comparison on the NeRF synthetic 360°
dataset. We report PSNR, SSIM, and LPIPS of previous methods
and ours on the NeRF Synthetic dataset. Note that "better render-
ing" setting of NeRF2Mesh is denoted by "R" and "better mesh"
by "M".

	Disk Storage ↓	Training Time ↓
MobileNeRF [9]	125.7 MB	20-24 h
Re-ReND [44]	198.4 MB	55-60 h
NeRF2Mesh [47]	73.5 MB	1-2 h
Ours	**46.9 MB**	1-2 h

Table 3. Comparison of disk storage and training time. We report
the size (MB) of the exported models and the training time (hour).

PSNR, SSIM, and LPIPS as the evaluation metrics. The ex-
periments are conducted on the NeRF synthetic dataset [32].
As shown in Table 2, our method generates comparable re-
sults with previous methods. It is worth noting that our pro-
posed method yields superior outcomes compared to pre-
vious approaches in terms of generating a smooth mesh.
Moreover, our approach generates comparable results with
methods that prioritize rendering over mesh quality.

Efficiency. In terms of model efficiency, we compare the
disk storage and the training time of our method and ex-
isting methods [9, 44, 47]. For a fair comparison, all the

models are trained on a single Tesla-V100 (32G) and the
disk storage consists of the uncompressed mesh file (.obj
and .mtl), texture file (.png), and the final model file (.json).
As shown in Table 3, our method consumes smaller disk
storage than previous methods. This can be attributed to the
utilization of an accurate surface-based model, which pre-
vents the generation of redundant vertices and faces. Ad-
ditionally, our approach incorporates a lightweight learn-
able texture in the rendering process, further reducing the
overall storage. As for the model training time, our method
achieves a much faster training speed than MobileNeRF [9]
and Re-ReND [44]. With the incorporation of the learn-
able implicit texture, our method directly optimizes the fi-
nal texture required for rendering and bypasses the exces-
sive computation required by these methods [9, 44] to trans-
form the sampling features from the radiance field to the
final textures. As for NeRF2Mesh [47], since it utilizes a
fast-training NeRF model before obtaining the mesh and
texture, it trains slightly faster than our method. How-
ever, our model can handle view-dependent surfaces that
NeRF2Mesh [47] could not with comparable training time.

Overall, EvaSurf exhibits high-fidelity rendering results
and generates more accurate mesh than previous methods.
Furthermore, from the perspective of real-world applica-
tions, EvaSurf is more suitable as it requires much less
disk storage and training time, which could reduce the con-
straints for hardware, and can render realistic results and
generate accurate mesh in real-time on mobile devices.

4.3. Comparisons on real-world 3D Objects

As depicted in Fig. 5, we also compare our rendering results
and mesh results with NeRF2Mesh [47] on a real-world
dataset. We train NeRF2Mesh under two settings following
the authors' instructions. We first train NeRF2Mesh under
the "better rendering" setting and extract the mesh named
"N2M Mesh-R" in the figure. Then we train it under the

CD: 5.33   CD: 5.48

Ground Truth   **w/ Progressive grids $g(\beta)$**   **w/o Progressive grids $g(\beta)$**
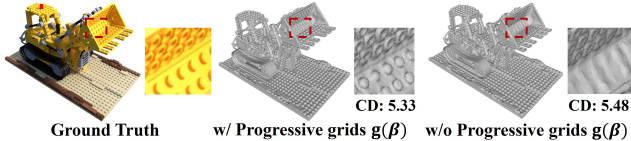
Figure 6. Ablation of the Progressive Grids. By utilizing a set of progressive grids, we could generate a mesh with better details. Chamfer Distance (CD ↓, unit is 10^{-3}) is provided as reference.

	CD ↓ (unit: 10^{-3})
w/ Progressive grids $g(\beta)$	**4.39**
w/o Progressive grids $g(\beta)$	5.35

Table 4. Comparison of Chamfer Distance (CD) results. We report the evaluation results of utilizing progressive grids or not in the surface-based model.

"better mesh" settings and extract the mesh named as "N2M Mesh-M", the renderings are generated correspondingly.

From the perspective of **geometry quality**, the "better mesh" setting of NeRF2Mesh generates a smoother surface than the "better rendering" setting but fails to reconstruct complex structures. On the other hand, using the "better rendering" setting and decimating the mesh size could obtain a better shape but the surface appears to be not smooth. This originates from the exportation methodology of NeRF-based model, which is incapable of reconstructing smooth complex surfaces. Contrarily, our method employs an explicit representation and utilizes a multi-view supervision module and a set of progressive grids to optimize the mesh. This allows our model to generate accurate surfaces effectively for these complex structures. From the perspective of **rendering quality**, our method achieves better appearances than NeRF2Mesh [47] under both the "better rendering" setting and "better mesh" setting. NeRF2Mesh directly bakes the appearance of the NeRF model into texture, which cannot render images with view-dependent effects. Meanwhile, we optimize a learnable implicit texture with a set of Gaussian lobes. By modeling view dependence with different fidelity in the feature space, our model can generate high-fidelity renderings for inputs with specularities.

4.4. Ablation Studies

Progressive Grids. Progressive grids with multi-resolution are employed in the surface-based model to realize the coarse-to-fine training strategy for better details. The effectiveness of these progressive grids is demonstrated in Fig. 6. We observe that a coarse shape is initialized when using low-resolution grids, while high-frequency details can be captured when using high-resolution grids. As demonstrated in Table 4, utilizing progressive grids in our surface-based model can lead to improved mesh quality.

Multi-view Supervision Module. By explicitly initializ-

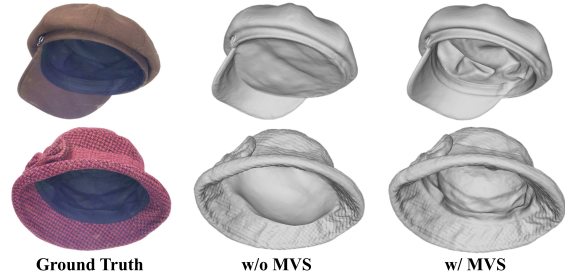

Ground Truth   **w/o MVS**   **w/ MVS**

Figure 7. Ablation of the Multiview Supervision Module (MVS). Note that the figure on the first column is relighted for a better view of the object's inner structure. It could be seen that we could reconstruct the interior structure of the hat with the aid of MVS.

	PSNR ↑	SSIM ↑	LPIPS ↓
w $L(f, v_{cos})$	**27.58**	**0.891**	**0.208**
w/o $L(f, v_{cos})$	26.69	0.884	0.215

Table 5. Ablation of view-dependent Gaussian lobes L. The model equipped with the Gaussian lobes exhibits better view-dependent rendering results.

ing the geometry with an additional multi-view supervision module, our method establishes a solid foundation for generating an accurate mesh. To better present the effectiveness of the multi-view supervision module, we compare the mesh results, shown in Fig. 7. For the same object, it could be seen that with the additional MVS, our method reconstructs a more accurate mesh with better details. The model without the additional MVS is not capable of reconstructing the mesh with complex structures such as the interior structure of a hat which contains several wrinkles. Meanwhile, with the additional supervision provided by MVS, our model manages to generate an accurate and well-structured mesh that matches the ground-truth images.

View-dependent Gaussian Lobes. In our real-time 3D object reconstruction method, we optimize a 12-dimensional learnable implicit texture to render high-fidelity images on various devices. To incorporate the view-dependent condition during optimization, we equip a set of Gaussian lobes to the original implicit texture. By modeling the view dependence with different fidelity, several view-dependent effects can be rendered by our method. The results on the real-world dataset are demonstrated in Table 5. It could be seen that we obtain better renderings with the set of Gaussian lobes. Since some regions are observable from only a limited range of viewing directions, modeling the view dependence with the same fidelity would lead to an average appearance aggregated from input views. By utilizing the Gaussian lobes L, we model the view-dependent information with different fidelity. By assigning different weights to each dimension of the texture in the feature space, we enable the model to reflect more realistic results.

5. Conclusion

In conclusion, we propose a novel method, EvaSurf, an efficient view-aware implicit textured surface reconstruction method on mobile devices. We first introduce a multi-view supervision to the surface-based model for the reconstruction of accurate mesh. We then equip a learnable implicit texture with a set of Gaussian lobes to render high-fidelity images with view-dependent effects. A neural shader, which is a lightweight MLP, is further employed to enable real-time rendering on mobile devices. Our approach is not limited to synthetic data but also manages to render real-world objects with high-quality appearance and accurate mesh. With the power of fast training and small disk storage, our method is capable of rendering on mobile devices at interactive frame rates without compromising on the quality of the output, generalized for daily applications.

References

[1] Daniel Andersen, Peter Villano, and Voicu Popescu. AR HMD guidance for controlled hand-held 3d acquisition. *IEEE Trans. Vis. Comput. Graph.*, 25(11):3073–3082, 2019. 2

[2] Jonathan T. Barron, Ben Mildenhall, Matthew Tancik, Peter Hedman, Ricardo Martin-Brualla, and Pratul P. Srinivasan. Mip-nerf: A multiscale representation for anti-aliasing neural radiance fields. In *ICCV*, pages 5835–5844, 2021. 2, 4

[3] Jonathan T. Barron, Ben Mildenhall, Dor Verbin, Pratul P. Srinivasan, and Peter Hedman. Mip-nerf 360: Unbounded anti-aliased neural radiance fields. In *CVPR*, pages 5460–5469, 2022. 2

[4] Jonathan T. Barron, Ben Mildenhall, Dor Verbin, Pratul P. Srinivasan, and Peter Hedman. Zip-nerf: Anti-aliased grid-based neural radiance fields. In *ICCV*, pages 19697–19705, 2023. 2

[5] David Blumenthal-Barby and Peter Eisert. High-resolution depth for binocular image-based modeling. *Comput. Graph.*, 39:89–100, 2014. 2

[6] Neill D. F. Campbell, George Vogiatzis, Carlos Hernández, and Roberto Cipolla. Using multiple hypotheses to improve depth-maps for multi-view stereo. In *ECCV*, pages 766–779, 2008. 2

[7] Anpei Chen, Zexiang Xu, Andreas Geiger, Jingyi Yu, and Hao Su. Tensorf: Tensorial radiance fields. In *ECCV*, pages 333–350, 2022. 2

[8] Wenzheng Chen, Huan Ling, Jun Gao, Edward J. Smith, Jaakko Lehtinen, Alec Jacobson, and Sanja Fidler. Learning to predict 3d objects with an interpolation-based differentiable renderer. In *NeurIPS*, pages 9605–9616, 2019. 2

[9] Zhiqin Chen, Thomas A. Funkhouser, Peter Hedman, and Andrea Tagliasacchi. Mobilenerf: Exploiting the polygon rasterization pipeline for efficient neural field rendering on mobile architectures. In *CVPR*, pages 16569–16578, 2023. 2, 3, 4, 5, 6, 7

[10] Carlos Hernández Esteban and Francis Schmitt. Silhouette and stereo fusion for 3d object modeling. In *3DIM*, pages 46–53, 2003. 2

[11] Sara Fridovich-Keil, Alex Yu, Matthew Tancik, Qinhong Chen, Benjamin Recht, and Angjoo Kanazawa. Plenoxels: Radiance fields without neural networks. In *CVPR*, pages 5491–5500, 2022. 3

[12] Sara Fridovich-Keil, Giacomo Meanti, Frederik Rahbæk Warburg, Benjamin Recht, and Angjoo Kanazawa. K-planes: Explicit radiance fields in space, time, and appearance. In *CVPR*, pages 12479–12488, 2023. 2

[13] Qiancheng Fu, Qingshan Xu, Yew Soon Ong, and Wenbing Tao. Geo-neus: Geometry-consistent neural implicit surfaces learning for multi-view reconstruction. In *NeurIPS*, 2022. 3

[14] Pascal Fua and Yvan G. Leclerc. Object-centered surface reconstruction: Combining multi-image stereo and shading. *Int. J. Comput. Vis.*, 16(1):35–56, 1995. 2

[15] Silvano Galliani, Katrin Lasinger, and Konrad Schindler. Massively parallel multiview stereopsis by surface normal diffusion. In *ICCV*, pages 873–881, 2015. 2

[16] Stephan J. Garbin, Marek Kowalski, Matthew Johnson, Jamie Shotton, and Julien P. C. Valentin. Fastnerf: High-fidelity neural rendering at 200fps. In *ICCV*, pages 14326–14335, 2021. 2

[17] Peter Hedman, Pratul P. Srinivasan, Ben Mildenhall, Jonathan T. Barron, and Paul E. Debevec. Baking neural radiance fields for real-time view synthesis. In *ICCV*, pages 5855–5864, 2021. 2, 3, 6, 7

[18] Jingwei Huang, Angela Dai, Leonidas J. Guibas, and Matthias Nießner. 3dlite: towards commodity 3d scanning for content creation. *ACM Trans. Graph.*, 36(6):203:1–203:14, 2017. 2

[19] Chiyu ”Max” Jiang, Avneesh Sud, Ameesh Makadia, Jingwei Huang, Matthias Nießner, and Thomas A. Funkhouser. Local implicit grid representations for 3d scenes. In *CVPR*, pages 6000–6009, 2020. 2

[20] Samuli Laine, Janne Hellsten, Tero Karras, Yeongho Seol, Jaakko Lehtinen, and Timo Aila. Modular primitives for high-performance differentiable rendering. *ACM Trans. Graph.*, 39(6):194:1–194:14, 2020. 5

[21] Zhaoshuo Li, Thomas Müller, Alex Evans, Russell H. Taylor, Mathias Unberath, Ming-Yu Liu, and Chen-Hsuan Lin. Neuralangelo: High-fidelity neural surface reconstruction. In *CVPR*, pages 8456–8465, 2023. 3

[22] Yiyi Liao, Simon Donné, and Andreas Geiger. Deep marching cubes: Learning explicit surface representations. In *CVPR*, pages 2916–2925, 2018. 2

[23] Chen-Hsuan Lin, Oliver Wang, Bryan C. Russell, Eli Shechtman, Vladimir G. Kim, Matthew Fisher, and Simon Lucey. Photometric mesh optimization for video-aligned 3d object reconstruction. In *CVPR*, pages 969–978, 2019. 2

[24] Shichen Liu, Weikai Chen, Tianye Li, and Hao Li. Soft rasterizer: A differentiable renderer for image-based 3d reasoning. In *ICCV*, pages 7707–7716, 2019. 2

[25] Zheng-Ning Liu, Yan-Pei Cao, Zheng-Fei Kuang, Leif Kobbelt, and Shi-Min Hu. High-quality textured 3d shape reconstruction with cascaded fully convolutional networks. *IEEE Trans. Vis. Comput. Graph.*, 27(1):83–97, 2021. 2

[26] Stephen Lombardi, Tomas Simon, Jason M. Saragih, Gabriel Schwartz, Andreas M. Lehrmann, and Yaser Sheikh. Neural volumes: learning dynamic renderable volumes from images. *ACM Trans. Graph.*, 38(4):65:1–65:14, 2019. 2

[27] Guillaume Loubet, Nicolas Holzschuch, and Wenzel Jakob. Reparameterizing discontinuous integrands for differentiable rendering. *ACM Trans. Graph.*, 38(6):228:1–228:14, 2019.

[28] Fujun Luan, Shuang Zhao, Kavita Bala, and Zhao Dong. Unified shape and SVBRDF recovery using differentiable monte carlo rendering. *Comput. Graph. Forum*, 40(4):101–113, 2021.

[29] Jiahui Lyu, Bojian Wu, Dani Lischinski, Daniel Cohen-Or, and Hui Huang. Differentiable refraction-tracing for mesh reconstruction of transparent objects. *ACM Trans. Graph.*, 39(6):195:1–195:13, 2020.

[30] Ricardo Martin-Brualla, Noha Radwan, Mehdi S. M. Sajjadi, Jonathan T. Barron, Alexey Dosovitskiy, and Daniel Duckworth. Nerf in the wild: Neural radiance fields for unconstrained photo collections. In *CVPR*, pages 7210–7219, 2021. 2

[31] Lars M. Mescheder, Michael Oechsle, Michael Niemeyer, Sebastian Nowozin, and Andreas Geiger. Occupancy networks: Learning 3d reconstruction in function space. In *CVPR*, pages 4460–4470, 2019. 3

[32] Ben Mildenhall, Pratul P. Srinivasan, Matthew Tancik, Jonathan T. Barron, Ravi Ramamoorthi, and Ren Ng. Nerf: Representing scenes as neural radiance fields for view synthesis. In *ECCV*, 2020. 2, 5, 6, 7

[33] Thomas Müller, Alex Evans, Christoph Schied, and Alexander Keller. Instant neural graphics primitives with a multiresolution hash encoding. *ACM Trans. Graph.*, 41(4):102:1–102:15, 2022. 2

[34] Jacob Munkberg, Wenzheng Chen, Jon Hasselgren, Alex Evans, Tianchang Shen, Thomas Müller, Jun Gao, and Sanja Fidler. Extracting triangular 3d models, materials, and lighting from images. In *CVPR*, pages 8270–8280, 2022. 2, 5, 6

[35] Michael Niemeyer and Andreas Geiger. GIRAFFE: representing scenes as compositional generative neural feature fields. In *CVPR*, pages 11453–11464, 2021. 2

[36] Michael Niemeyer, Lars M. Mescheder, Michael Oechsle, and Andreas Geiger. Differentiable volumetric rendering: Learning implicit 3d representations without 3d supervision. In *CVPR*, pages 3501–3512, 2020. 2, 3

[37] Michael Oechsle, Songyou Peng, and Andreas Geiger. UNISURF: unifying neural implicit surfaces and radiance fields for multi-view reconstruction. In *ICCV*, pages 5569–5579, 2021. 3

[38] Keunhong Park, Utkarsh Sinha, Jonathan T. Barron, Sofien Bouaziz, Dan B. Goldman, Steven M. Seitz, and Ricardo Martin-Brualla. Nerfies: Deformable neural radiance fields. In *ICCV*, pages 5845–5854, 2021. 2

[39] Songyou Peng, Michael Niemeyer, Lars M. Mescheder, Marc Pollefeys, and Andreas Geiger. Convolutional occupancy networks. In *ECCV*, pages 523–540, 2020. 3

[40] Albert Pumarola, Enric Corona, Gerard Pons-Moll, and Francesc Moreno-Noguer. D-nerf: Neural radiance fields for dynamic scenes. In *CVPR*, pages 10318–10327, 2021. 2

[41] Marie-Julie Rakotosaona, Fabian Manhardt, Diego Martin Arroyo, Michael Niemeyer, Abhijit Kundu, and Federico Tombari. Nerfmeshing: Distilling neural radiance fields into geometrically-accurate 3d meshes. In *International Conference on 3D Vision (3DV)*, 2023. 3

[42] Christian Reiser, Songyou Peng, Yiyi Liao, and Andreas Geiger. Kilonerf: Speeding up neural radiance fields with thousands of tiny mlps. In *ICCV*, pages 14315–14325, 2021. 2

[43] Christian Reiser, Richard Szeliski, Dor Verbin, Pratul P. Srinivasan, Ben Mildenhall, Andreas Geiger, Jonathan T. Barron, and Peter Hedman. MERF: memory-efficient radiance fields for real-time view synthesis in unbounded scenes. *ACM Trans. Graph.*, 42(4):89:1–89:12, 2023. 2

[44] Sara Rojas, Jesus Zarzar, Juan C. Pérez, Artsiom Sanakoyeu, Ali Thabet, Albert Pumarola, and Bernard Ghanem. Re-rend: Real-time rendering of nerfs across devices. In *ICCV*, pages 3632–3641, 2023. 2, 3, 4, 5, 6, 7

[45] Tianchang Shen, Jun Gao, Kangxue Yin, Ming-Yu Liu, and Sanja Fidler. Deep marching tetrahedra: a hybrid representation for high-resolution 3d shape synthesis. In *NeurIPS*, pages 6087–6101, 2021. 2

[46] Pratul P. Srinivasan, Boyang Deng, Xiuming Zhang, Matthew Tancik, Ben Mildenhall, and Jonathan T. Barron. Nerv: Neural reflectance and visibility fields for relighting and view synthesis. In *CVPR*, pages 7495–7504, 2021. 2

[47] Jiaxiang Tang, Hang Zhou, Xiaokang Chen, Tianshu Hu, Errui Ding, Jingdong Wang, and Gang Zeng. Delicate textured mesh recovery from nerf via adaptive surface refinement. In *ICCV*, pages 17739–17749, 2023. 2, 3, 4, 5, 6, 7, 8

[48] Justus Thies, Michael Zollhöfer, and Matthias Nießner. Deferred neural rendering: image synthesis using neural textures. *ACM Trans. Graph.*, 38(4):66:1–66:12, 2019. 3

[49] Justus Thies, Michael Zollhöfer, Christian Theobalt, Marc Stamminger, and Matthias Nießner. Image-guided neural object rendering. In *ICLR*, 2020. 3

[50] Engin Tola, Christoph Strecha, and Pascal Fua. Efficient large-scale multi-view stereo for ultra high-resolution image sets. *Mach. Vis. Appl.*, 23(5):903–920, 2012. 2

[51] Dor Verbin, Peter Hedman, Ben Mildenhall, Todd E. Zickler, Jonathan T. Barron, and Pratul P. Srinivasan. Ref-nerf: Structured view-dependent appearance for neural radiance fields. In *CVPR*, pages 5481–5490, 2022. 2

[52] Delio Vicini, Sébastien Speierer, and Wenzel Jakob. Differentiable signed distance function rendering. *ACM Trans. Graph.*, 41(4):125:1–125:18, 2022. 3

[53] Hoang-Hiep Vu, Patrick Labatut, Jean-Philippe Pons, and Renaud Keriven. High accuracy and visibility-consistent dense multiview stereo. *IEEE Trans. Pattern Anal. Mach. Intell.*, 34(5):889–901, 2012. 2

[54] Peng Wang, Lingjie Liu, Yuan Liu, Christian Theobalt, Taku Komura, and Wenping Wang. Neus: Learning neural implicit surfaces by volume rendering for multi-view reconstruction. In *NeurIPS*, pages 27171–27183, 2021. 3, 4, 5, 6

[55] Qianqian Wang, Zhicheng Wang, Kyle Genova, Pratul P. Srinivasan, Howard Zhou, Jonathan T. Barron, Ricardo

Martin-Brualla, Noah Snavely, and Thomas Funkhouser. Ibrnet: Learning multi-view image-based rendering. In *CVPR*, pages 4690–4699, 2021. 3

[56] Zirui Wang, Shangzhe Wu, Weidi Xie, Min Chen, and Victor Adrian Prisacariu. Nerf–: Neural radiance fields without known camera parameters. *arXiv preprint arXiv:2102.07064*, 2021. 2

[57] Chao Wen, Yinda Zhang, Zhuwen Li, and Yanwei Fu. Pixel2mesh++: Multi-view 3d mesh generation via deformation. In *ICCV*, pages 1042–1051, 2019. 2

[58] Chao Wen, Yinda Zhang, Chenjie Cao, Zhuwen Li, Xiangyang Xue, and Yanwei Fu. Pixel2mesh++: 3d mesh generation and refinement from multi-view images. *IEEE Trans. Pattern Anal. Mach. Intell.*, 45(2):2166–2180, 2023. 2

[59] Tong Wu, Jiaqi Wang, Xingang Pan, Xudong Xu, Christian Theobalt, Ziwei Liu, and Dahua Lin. Voxurf: Voxel-based efficient and accurate neural surface reconstruction. In *ICLR*, 2023. 3

[60] Lior Yariv, Yoni Kasten, Dror Moran, Meirav Galun, Matan Atzmon, Ronen Basri, and Yaron Lipman. Multiview neural surface reconstruction by disentangling geometry and appearance. In *NeurIPS*, 2020.

[61] Lior Yariv, Jiatao Gu, Yoni Kasten, and Yaron Lipman. Volume rendering of neural implicit surfaces. In *NeurIPS*, pages 4805–4815, 2021. 3

[62] Lior Yariv, Peter Hedman, Christian Reiser, Dor Verbin, Pratul P. Srinivasan, Richard Szeliski, Jonathan T. Barron, and Ben Mildenhall. Bakedsdf: Meshing neural sdfs for real-time view synthesis. In *SIGGRAPH*, pages 46:1–46:9, 2023. 2, 3

[63] Alex Yu, Ruilong Li, Matthew Tancik, Hao Li, Ren Ng, and Angjoo Kanazawa. Plenoctrees for real-time rendering of neural radiance fields. In *ICCV*, pages 5732–5741, 2021. 3

[64] Alex Yu, Vickie Ye, Matthew Tancik, and Angjoo Kanazawa. pixelnerf: Neural radiance fields from one or few images. In *CVPR*, pages 4578–4587, 2021. 2

[65] Zehao Yu, Songyou Peng, Michael Niemeyer, Torsten Sattler, and Andreas Geiger. Monosdf: Exploring monocular geometric cues for neural implicit surface reconstruction. In *NeurIPS*, 2022. 3

[66] Kai Zhang, Gernot Riegler, Noah Snavely, and Vladlen Koltun. Nerf++: Analyzing and improving neural radiance fields. *arXiv preprint arXiv:2010.07492*, 2020. 2

[67] Xiuming Zhang, Pratul P. Srinivasan, Boyang Deng, Paul E. Debevec, William T. Freeman, and Jonathan T. Barron. Nerfactor: neural factorization of shape and reflectance under an unknown illumination. *ACM Trans. Graph.*, 40(6):237:1–237:18, 2021. 2